An Approach to Estimate the Areal Rain-Rate Distribution from Spaceborne Radar by the Use of Multiple Thresholds

R. MENEGHINI

NASA/Goddard Space Flight Center, Greenbelt, Maryland

J. A. JONES

Hughes STX Corporation, Lanham, Maryland

(Manuscript received 18 June 1991, in final form 6 April 1992)

ABSTRACT

Estimates of rain rate derived from a spaceborne weather radar will be most reliable over an intermediate range of values. At light or heavy rain rates, where the signal-to-noise ratios are degraded either by small values of the backscattered power or by large attenuation, the accuracy will be poor. In forming an area average of the rain rate, an alternative to the averaging of the high-resolution estimates, irrespective of their individual accuracies, is a multiple threshold approach. The method is based on the fact that the fractional area above a particular rain-rate threshold R_j is related to the cumulative distribution of rain rates evaluated at R_j. Varying the threshold over the effective dynamic range of the radar yields the cumulative distribution function over this range. To obtain the distribution at all rain rates, a lognormal or gamma test function is selected such that the mean-square error between the test function and the measured values is minimized. Once the unknown parameters are determined, the first-order statistics of the areawide rain-rate distribution can be found. Tests of the method with data from the SPANDAR radar provide comparisons between it and the single threshold and the direct averaging approaches.

1. Introduction and background

Methods that relate the fractional-area coverage of rain rate over a certain threshold to the area-average rain rate have been shown to be quite good with regard to the high degree of correlation between the two quantities and the applicability of the method to different climatological regions (Chiu 1988; Kedem et al. 1990; Rosenfeld et al. 1990; Atlas et al. 1990; Short et al. 1992). Early work in this field was concerned primarily with the volumetric rainfall R and its relation to the area–time integral (ATI), defined as the temporal and spatial integration of the area over which the rain rate (or dBZ value) exceeds a fixed threshold (Byers 1948; Donneaud et al. 1984).

Much of the recent work can be viewed as the ATI method with the temporal integration (summation) reduced to a single, areawide observation. The fact that high correlations persist between the fractional area coverage above a threshold and the instantaneous area-average rain rate is a significant new observation that can not be inferred from the time-averaged results.[1]

Atlas et al. (1990) have argued that the strength of this correlation rests on the fact that the probability distribution of rain rate over large areas is fairly stable over time and space. For this to be the case, the area must be sufficiently large to include storm cells at various stages of their life cycle so that a single "snapshot" of the fractional-area coverage serves as a good indicator of the average rain rate. Starting from the assumption that the rain rate R follows a mixed distribution consisting of a discrete and a continuous component, Kedem et al. (1990) have shown that the mean value can be expressed as a product of a "slope" parameter β and the probability that R exceeds some fixed threshold. The parameter β, moreover, depends only on the continuous (nonzero) part of the rain-rate dis-

Corresponding author address: R. Meneghini, NASA/Goddard Space Flight Center, Code 975, Greenbelt, MD 20771.

[1] The relationship between the two methods is analogous to that between the integrals of functions and the functions themselves. In particular, in the equations (i) $f(x) = g(x)$ and (ii) $\int f(x)dx = \int g(x)dx$, (i) implies (ii) but not conversely. In an analogous fashion, high correlations in the "instantaneous ATI" guarantee high correlations in the time average but not conversely.

tribution so that if this is relatively stable over large areas, this single parameter can be used to specify the distribution. In an earlier study, Chiu (1988), using the GARP (Global Atmospheric Research Program) Atlantic Tropical Experiment (GATE) datasets, found the correlation between fractional-area coverage and rain rate to be maximized for thresholds at about 5 mm h^{-1}. He noted that this level corresponds to the separation between convective (rain rates greater than 5 mm h^{-1}) and stratiform rain (rain rates less than 5 mm h^{-1}), so that, at least in this instance, the thresholding method functions in a manner similar to the visible–infrared techniques. Analyses of other datasets have shown that the optimum threshold is not constant but varies with location (Rosenfeld et al. 1990; Short et al. 1993).

These studies indicate that a single rain-rate threshold, if properly chosen, can be used to estimate the area-average rain rate quite accurately if the area is large. On the other hand, if the sensor were perfect in the sense that it could measure the rain rate exactly over the full dynamic range, we could not only dispense with such methods but recover the complete distribution function of rain rate over any area of interest. In practice, the situation is somewhere between these two extremes: while the radar can measure more than the fractional-area coverage at a single threshold, the instruments are limited to a finite dynamic range and subject to instrument noise, attenuation effects, and a host of other problems. In this study, we analyze a simplified version of this intermediate situation, appropriate to spaceborne radars in particular, by assuming that the instrument provides a perfect measurement over a finite dynamic range. Within this range of measurable rain rates, the idea of multiple thresholds is used to estimate the distribution function. To recover the distribution at all rain rates, a model function is chosen with the unknown parameters adjusted so that the mean-square error between the test function and the measured values of the distribution function is minimized. Once the unknown parameters are obtained and the test function fully specified, the first-order statistics of the distribution can be derived. Some of the questions of interest are: how does the accuracy of this multiple-threshold procedure compare with that of the single-threshold approach; how well can the distribution of rain rates be estimated that exceed the dynamic range of the instrument; and finally, what is the relationship between the instrument performance and the accuracy of the statistical characterization of rain rate?

2. Approach

In the application of the multiple-threshold procedure, the instrument is assumed to provide a perfect measurement of the rain rate but over a finite dynamic range from $R_T(1)$ to $R_T(n)$. Although this model is highly idealized, it is a reasonable first approximation to a spaceborne weather radar that is usually limited at the low rain rates by small signal-to-noise ratios and at high rain rates by attenuation effects. A second reason for using this model is to focus on basic idea of multiple thresholding and its relation to the single-threshold approach. Since both methods are affected similarly by calibration offsets and errors in the Z–R law, their introduction is more of a distraction than a help. A discussion of errors under less idealized conditions is given in section 5.

The assumption that the rain rate is measured perfectly between $R_T(1)$ and $R_T(n)$ can be restated by saying that the fractional area coverage above a rain-rate threshold $R_T(j)$ can be determined exactly for any R falling between $R_T(1)$ and $R_T(n)$. To apply this assumption to a set of measurements, we begin with a plan position indicator (PPI) map from a ground-based radar and convert the radar reflectivities into rain rates. The resulting map is taken to be the true rain-rate field from which the distribution function of rain rates over the PPI can be derived. It is worth emphasizing that the errors arising from the conversion of the reflectivity factors to rain rates are not considered here and that these rain rates are simply used as the "true values" against which the results of the simulation can be checked.

To apply the thresholding procedure, it is convenient to think of "unwinding" the rain-rate PPI by mapping each concentric ring onto adjacent segments along a line. Next a family of functions $Y[R_T(j)]$, $j = 1, 2, \cdots, n$, is defined by

$$Y[R_T(j)] = Y_j = \begin{cases} 1, & R > R_T(j) \\ 0, & R < R_T(j). \end{cases} \quad (1)$$

Interpreting R, and therefore Y, as random variables, the expected value of Y_j is equal to the probability that the rain rate exceeds the threshold value $R_T(j)$ (Papoulis 1965). Since $\Pr[R > R_T(j)] = 1 - \Pr[R < R_T(j)]$, then

$$E(Y_j) = 1 - F[R_T(j)], \quad (2)$$

where $F[R_T(j)]$ is the probability distribution function of the rain rate R evaluated at $R = R_T(j)$. Although $F(R)$ will be referred to as a probability distribution function, the distribution that it characterizes is only that of the particular PPI and not the ensemble of rain rates over the area in question. Indeed, $F(R)$ is simply the integral from 0 to R of the normalized histogram of rain rates over the PPI.

Examples of Y_j are shown in Fig. 1. In Fig. 1a, the rain rate is plotted as a function of azimuth for a radar range centered at 25 km. These data were taken by the SPANDAR radar at Wallops Island, Virginia, from observations made on 17 November 1988. Figure 1

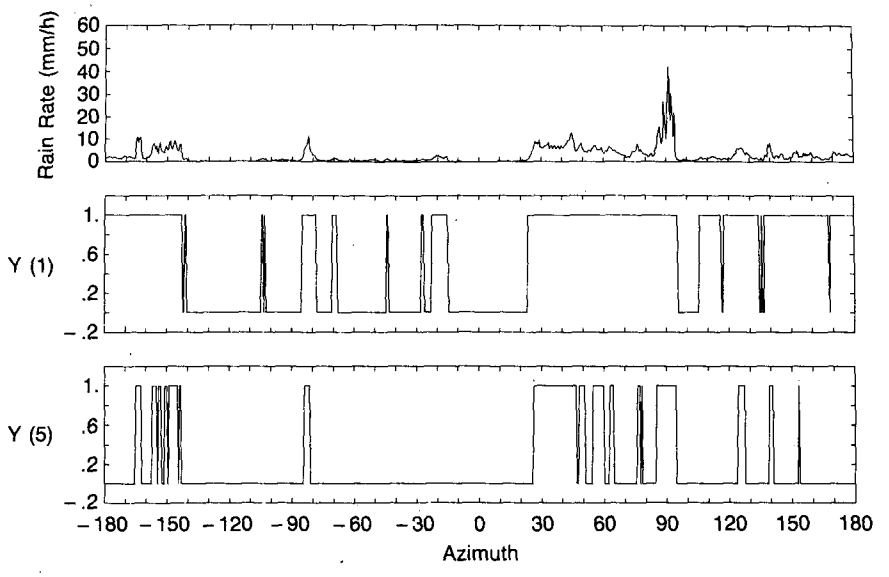

FIG. 1. (a) Rain rate versus azimuthal angle at a radar range of 25 km; (b) and (c) corresponding values of the threshold function Y at $R = 1$ mm h^{-1} and $R = 5$ mm h^{-1}, respectively.

shows only a portion of the function: the complete plot would consist of a concatenation of these azimuthal curves (suitably scaled to preserve the area) from the minimum (5 km) to the maximum range (130 km). Shown below the rain-rate curve in Fig. 1a are plots of the corresponding Y for rain-rate thresholds of 1 mm h^{-1} (Fig. 1b) and 5 mm h^{-1} (Fig. 1c). Taking the mean values of Y ($R_T = 1$ mm h^{-1}) and Y ($R_T = 5$ mm h^{-1}) and using (1) provides estimates of $F(R)$ at these rain rates.

By a simple extension of the procedure just described, $F(R)$ can be obtained for values of R that lie within the dynamic range of the instrument, that is, between $R_T(1)$ and $R_T(n)$. To specify $F(R)$ for all values of R, we use a model distribution function $F_m(R)$ of mixed type (Kedem et al. 1990) where the discontinuous part is given by a step function at $R = 0$ mm h^{-1} of strength $(1 - p)$, where p is the fractional area over which the rain rate is nonzero. The continuous portion of $F_m(R)$ is assumed to be either a lognormal or a gamma distribution. For the lognormal distribution, F_m is given by

$$F_m(R) = (1 - p)U(R) + \frac{p}{2}[1 + \Phi(u)] \quad (3)$$

for $R \geq 0$ and zero for $R < 0$ and where Φ is the error function, U the step function, and $u = (\ln R - m)(2^{0.5}s)^{-1}$. The mean and variance of R are given by

$$E(R) = p \exp\left(m + \frac{s^2}{2}\right) \quad (4)$$

$$\text{var}(R) = p[\exp(2m + s^2)][\exp(s^2) - p]. \quad (5)$$

When the continuous portion follows a gamma distribution, the test function for $R \geq 0$ becomes

$$F_m(R) = (1 - p)U(R) + \left[\frac{p}{\Gamma(\beta + 1)}\right]\gamma(\beta + 1, \alpha R), \quad (6)$$

where γ and Γ are the incomplete and complete gamma functions, respectively, where

$$\gamma(a, x) = \int_0^x e^{-t}t^{a-1}dt$$

$$\Gamma(a) = \gamma(a, \infty).$$

The corresponding mean and variance are

$$E(R) = \frac{p(\beta + 1)}{\alpha} \quad (7)$$

$$\text{var}(R) = p\left(\frac{\beta + 1}{\alpha}\right)^2[(\beta + 2) - p(\beta + 1)]. \quad (8)$$

The distribution, mean, and variance conditioned on $R > 0$ can be obtained from the above formulas by setting p equal to 1.

The procedure can be summarized as follows. Beginning with an instrument dynamic range from $R_T(1)$ to $R_T(n)$, the corresponding functions $Y[R_T(j)]$ ($j = 1, \cdots, n$) are computed and then used to calculate the value of the distribution $F(R)$ at $R = R_T(j)$. The unknown parameters of the model function $F_m(R)$ are found by minimizing the mean-square error between this function and the n values of $F[R_T(j)]$. Because the procedure provides $F_m(R)$ for all R, any first-order statistic of the areawide rain rate can be computed.

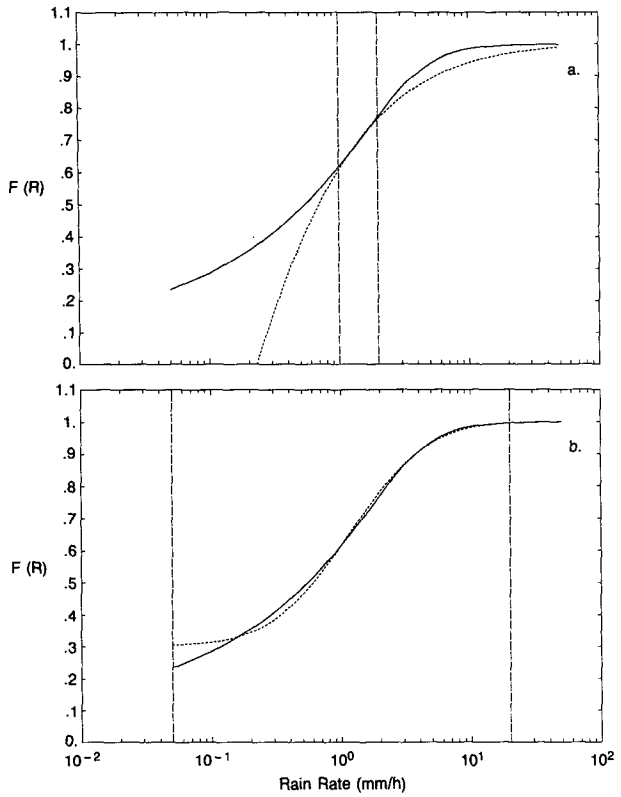

FIG. 2. Estimated probability distribution functions (dashed lines) for: (a) a narrow dynamic range of 1–2 mm h^{-1} and (b) a broad dynamic range of 0.05–20 mm h^{-1}. The actual distribution function is given by the solid lines.

3. Results

a. *Estimation of area-average rain rate*

Figure 2 shows two examples of the method for a single PPI SPANDAR radar map using the lognormal model given by (3). In each figure, the true rain-rate distribution function is given by the solid line: the corresponding mean and standard deviation of the areal rain rate are 1.47 and 3.17 mm h^{-1}, respectively. In Fig. 2a, the estimated distribution function for a dynamic range from 1 to 2 mm h^{-1} is shown by the dashed line. The corresponding mean and standard deviation of the rain rates, given by 4.53 and 113 mm h^{-1}, respectively, exhibit an extremely large error in the estimation. A shift in the dynamic range from 1 to 2 mm h^{-1} down to 0.5 to 1 mm h^{-1} provides an improvement in the estimated distribution so that the area-average rain rate reduces to 1.9 mm h^{-1} (not shown). By broadening the dynamic range to 0.05–20 mm h^{-1}, the estimated distribution yields $E(R) = 1.5$ mm h^{-1} and $\sigma(R) = 3.0$ mm h^{-1}, which are close to the actual statistics (Fig. 2b). Despite agreeing so well, Fig. 2b shows that the shapes of the estimated and actual distributions differ at low rain rates. This departure seems to be caused by the fact that at light rain rates the distribution is not well represented by the lognormal. As will be shown later, the gamma distribution generally provides a more accurate representation of the actual distributions at the lower rain rates.

Using the procedure described above, SPANDAR PPI maps from 4 days have been processed, giving a total

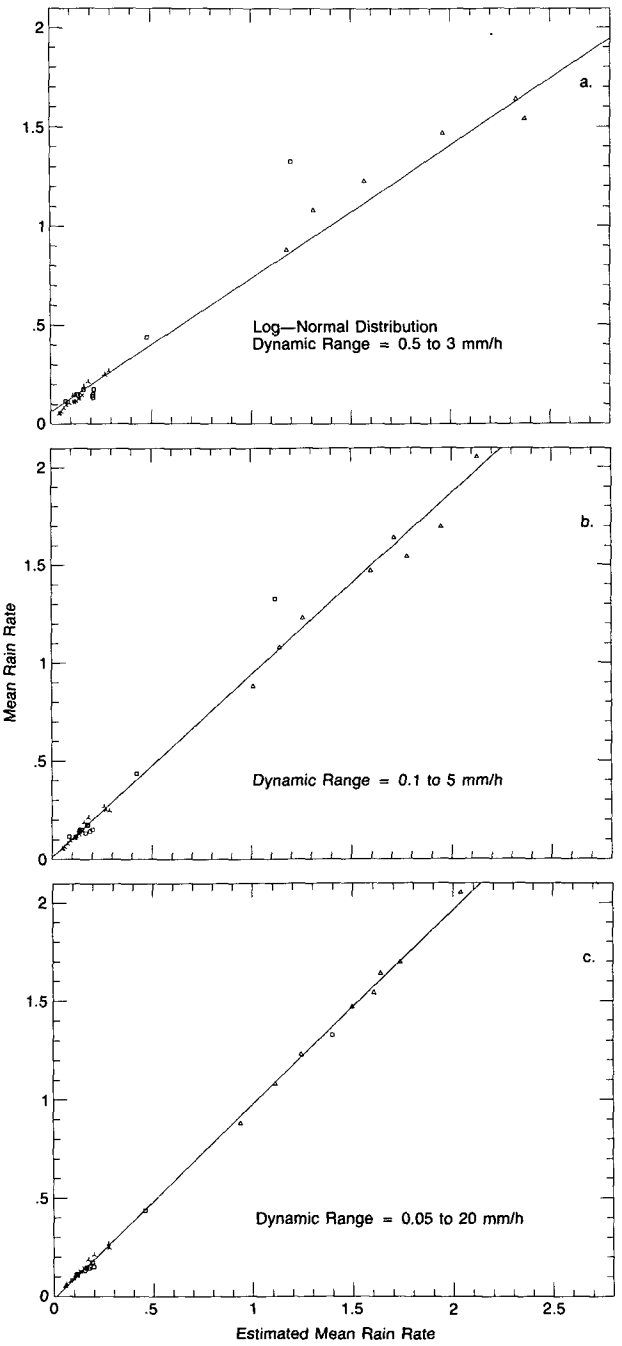

FIG. 3. Scatterplots of the true versus the estimated values of area mean rain rates for 37 SPANDAR PPI maps for three dynamic ranges using a lognormal distribution function.

of 37 maps. In all cases, the elevation angle is 0.5° with a range resolution of 0.6 km. Because of the narrow beamwidth of 0.4° and the radar frequency of 2.8 GHz, partial beam filling and attenuation should not be significant sources of error. On the other hand, radar calibration errors on the order of 2 dB and the use of the standard Z–R relationship $Z = 200R^{1.6}$ cause errors in the rain-rate estimates. As noted earlier, for the purpose of the present simulation, these errors are neglected and the statistics derived from the rain-rate maps are referred to as the true or actual values.

Plots of the actual versus the estimated area-average rain rates are shown in Fig. 3 for three dynamic ranges: 0.5–3 (Fig. 3a); 0.1–5 (Fig. 3b); and 0.05–20 mm h^{-1} (Fig. 3c). The statistics of these and two other cases are given in Table 1. In each case, the estimated mean values are obtained from a distribution function based on the mixed lognormal model (3). Note that the different symbols correspond to the day on which the PPI map was measured: examples from 17 November 1988 are represented by triangles, 14 June 1989 by squares, 21 June 1989 by an inverted Y, and 13 July 1989 by X. For the case where the dynamic range is most narrow (Table 1), a large positive bias in the estimate occurs. The situation improves dramatically when the dynamic range is increased from 0.5–1 to 0.5–3 mm h^{-1} (Fig. 3a), giving a smaller scatter and a regression line much closer to unity. Further improvement is obtained by increasing the dynamic range to 0.1–5 mm h^{-1} (Fig. 3b) and again to 0.05–20 mm h^{-1} (Fig. 3c), a span that covers the majority of the observed rain rates. It is worth noting that in this last case we can normally dispense with the test function and fitting procedure entirely and estimate the statistics based directly on the measured values of the distribution. We will return to this point in section 4 where the relative merits of local and statistical methods are discussed.

In Fig. 4, a similar set of plots is shown but under the assumption that the model distribution function is described by the mixed gamma (6). For narrow dynamic ranges, the estimated area-average rain rates derived from the gamma distribution are generally more accurate than those obtained from the lognormal. The largest difference occurs in the case of the smallest dynamic range (0.5–1 mm h^{-1}): for the lognormal model function, the square of the correlation coefficient ρ^2 is 0.67, while for the gamma model function, it is 0.96. Comparisons of the results are given in Table 1 for five values of the dynamic range. In addition to ρ^2, several other statistics are given: the mean-square error MSE, the standard error of estimate SEE, and the slope of the regression curve. It should be noted that although the estimated mean value has been plotted along the abscissa, the SEE and slope of the regression are computed by taking the estimate as the dependent variable and the actual value as the independent variable so that a slope greater than 1 corresponds to a positive bias in the estimate. The results of Table 1 show that under the lognormal test function, the estimates tend to be positively biased at the most narrow dynamic range (0.5–1 mm h^{-1}), but that this bias tends toward zero as the dynamic range is increased. By contrast, the results obtained from the gamma test function tend to be negatively biased. The trend toward progressively smaller biases exhibited in the lognormal case is not as obvious using the gamma test function where the slope of regression closest to one actually occurs at a narrow dynamic range.

b. *Comparisons with the single-threshold method*

Plots of the true area-average rain rate versus the fractional area coverage are shown in Fig. 5 for the threshold values of 0.2 (Fig. 5a), 1 (Fig. 5b), and 10 mm h^{-1} (Fig. 5c). Values of ρ^2 and SEE are given in Table 2 for five threshold rain rates. With the exception of the 10 mm h^{-1} threshold, ρ^2 exceeds 0.9 and attains a maximum of 0.984 at a threshold of 1 mm h^{-1}. Although these results are quite good, Table 1 shows that

TABLE 1. Statistics for the estimation of area-average rain rate using multiple thresholds (N = 37).

Dynamic range (mm h^{-1})	ρ^2	MSE (mm h^{-1})	SEE (mm h^{-1})	Slope
Lognormal distribution				
0.5–1	.667	9.000	5.150	12.00
0.5–3	.969	0.334	0.152	1.44
0.5–5	.987	0.093	0.073	1.08
0.1–5	.989	0.080	0.065	1.07
0.05–20	.999	0.027	0.020	1.01
Gamma distribution				
0.5–1	.955	0.252	0.169	1.31
0.5–3	.983	0.095	0.074	0.96
0.5–5	.990	0.094	0.056	0.92
0.1–5	.991	0.091	0.052	0.92
0.05–20	.999	0.047	0.016	0.95

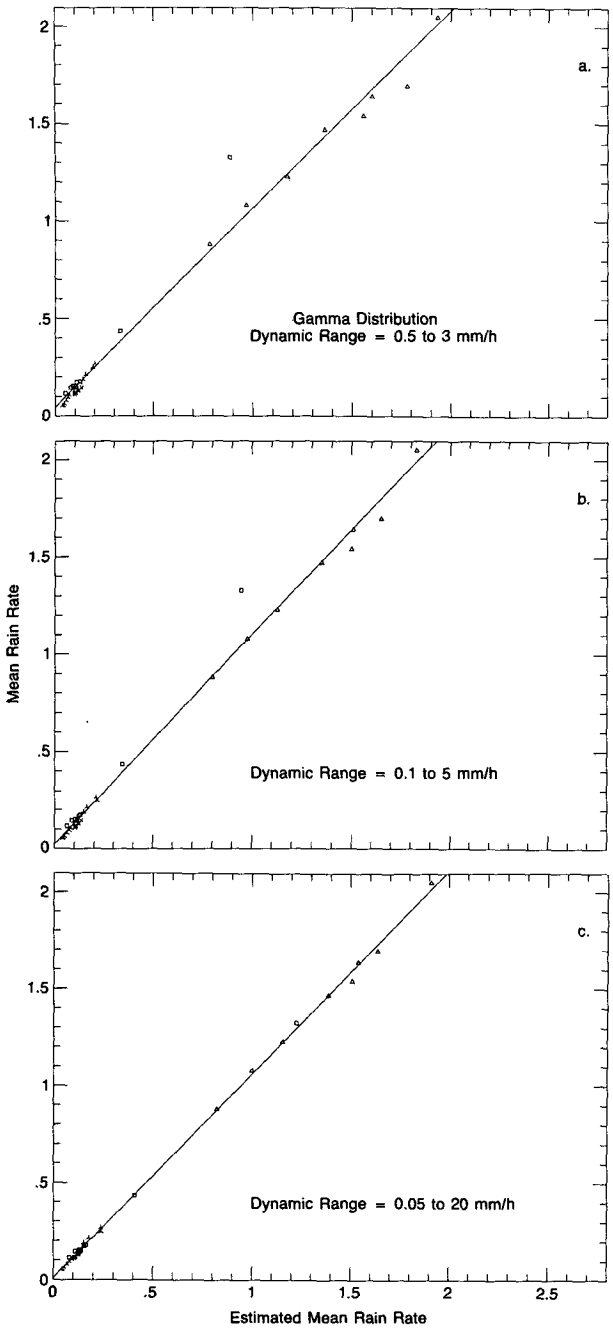

FIG. 4. Same as Fig. 3 but using a gamma model distribution function.

the multiple-threshold procedure yields more accurate estimates when the dynamic range is 0.5–5 mm h^{-1} or broader. On the other hand, for a dynamic range of 0.5–1 mm h^{-1}, a single threshold between 0.5 and 5 mm h^{-1} yields higher correlations and smaller scatter about the regression line than the use of multiple thresholds using either the lognormal or gamma test function. These results indicate that despite some superficial similarities, the single- and multiple-threshold methods are fundamentally different in terms of the approach, accuracy, and range of applicability. In particular, if multiple thresholding were a simple generalization of the single-threshold approach, we should expect the two methods to merge when the dynamic range is reduced to a single point. That the multiple-threshold approach fails when the dynamic range is

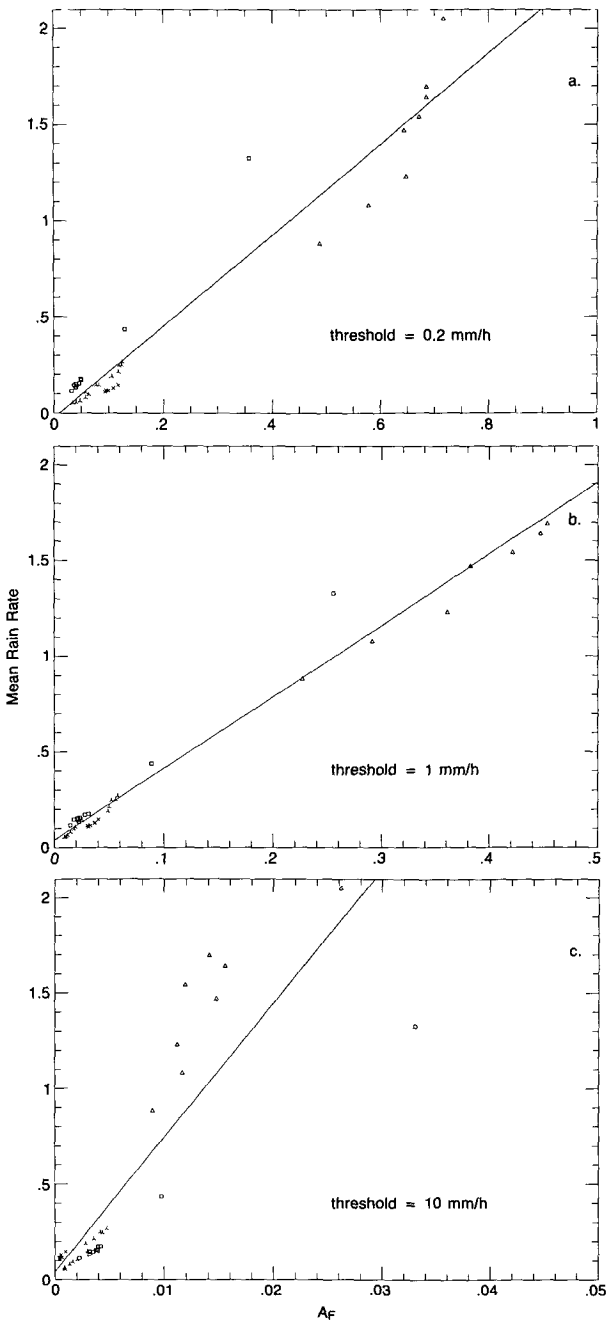

FIG. 5. Scatterplots of the mean area rain rate versus the fractional-area coverage A_F for three threshold rain rates.

TABLE 2. Statistics for the single-threshold method ($N = 37$).

Threshold (mm h^{-1})	ρ^2	SEE (mm h^{-1})
0.2	.939	0.147
0.5	.968	0.107
1	.984	0.075
5	.976	0.091
10	.759	0.291

TABLE 4. Single-threshold statistics: four partitions per map ($N = 128$).

Threshold (mm h^{-1})	ρ^2	SEE (mm h^{-1})
0.2	.740	0.403
0.5	.849	0.307
1	.913	0.233
5	.893	0.258
10	.605	0.496

reduced beyond a certain span indicates that a narrow range of values is insufficient to reconstruct the distribution function.

By decreasing the area, the accuracy of both methods is expected to degrade. We also expect to observe a rough equivalence between the dynamic range and the sampling area in the sense that maintaining a particular accuracy in the average rain-rate estimate over a shrinking area requires an increase in the dynamic range of the instrument. To examine these issues, each of the 37 PPI maps is divided into four equal areas and the single- and multiple-threshold methods are applied to each map after eliminating those sectors for which the fractional area coverage at a threshold of 0.2 mm h^{-1} is less than 2%. The results for the 128 cases are summarized in Tables 3 and 4 for the multiple- and single-threshold methods, respectively. Two cases are shown in Fig. 6: in the top (Fig. 6a), the mean rain rate versus the fractional-area coverage A_F is plotted for a single threshold of 1 mm h^{-1}; in the bottom, a scatterplot is shown of the true versus the estimated mean rain rate for multiple thresholds between 0.1 to 5 mm h^{-1}. Comparisons of the values in Tables 3 and 4 with the corresponding results in Tables 1 and 2 show in all cases that both ρ^2 and the SEE decrease with averaging area. For the single-threshold method, the reduction in area by a factor of 4 increases the SEE by about a factor of 3; for the multiple thresholds, the SEE increases by a factor of about 3.5 for the lognormal and by about 2.5 for the gamma distribution. A closer examination of the results in the tables shows that these approximations are crude, especially for the extreme cases of high thresholds and for the most narrow and broad dynamic ranges. A much larger database will be needed to establish a quantitative relationship among the variables of dynamic range, accuracy, and averaging area.

Although the accuracy of the methods degrades significantly with a reduction in area, the relative performance of the single- and multiple-threshold methods is unchanged. In particular, the use of multiple thresholds is preferable to a single threshold if the dynamic range is 0.5–5 mm h^{-1} or broader; the gamma test function is more accurate than the lognormal for most dynamic ranges but approximately the same (or slightly worse) for the broadest dynamic range. Finally, the gamma test function tends to yield negatively biased estimates, while the lognormal yields positively biased estimates.

c. *Statistics other than the area average*

Although the single-threshold method gives surprisingly high correlations between fractional area and area-average rain rate for thresholds between approximately 0.5 and 5 mm h^{-1}, the method is limited by two factors. To convert fractional area at a particular threshold to the area-average rain rate requires an independent estimate of rain rate. For a spaceborne sen-

TABLE 3. Multiple threshold statistics—area-average rain rate: four partitions per map ($N = 128$).

Dynamic range (mm h^{-1})	ρ^2	MSE (mm h^{-1})	SEE (mm h^{-1})	Slope
Lognormal distribution				
0.5–1	.080	$\gg 1$	$\gg 1$	$\gg 1$
0.5–3	.628	1.27	1.06	1.74
0.5–5	.921	0.293	0.261	1.13
0.1–5	.935	0.252	0.229	1.10
0.05–20	.991	0.084	0.077	1.01
Gamma distribution				
0.5–1	.530	1.740	1.510	2.030
0.5–3	.935	0.217	0.204	0.979
0.5–5	.966	0.176	0.135	0.915
0.1–5	.970	0.170	0.128	0.915
0.05–20	.990	0.010	0.074	0.949

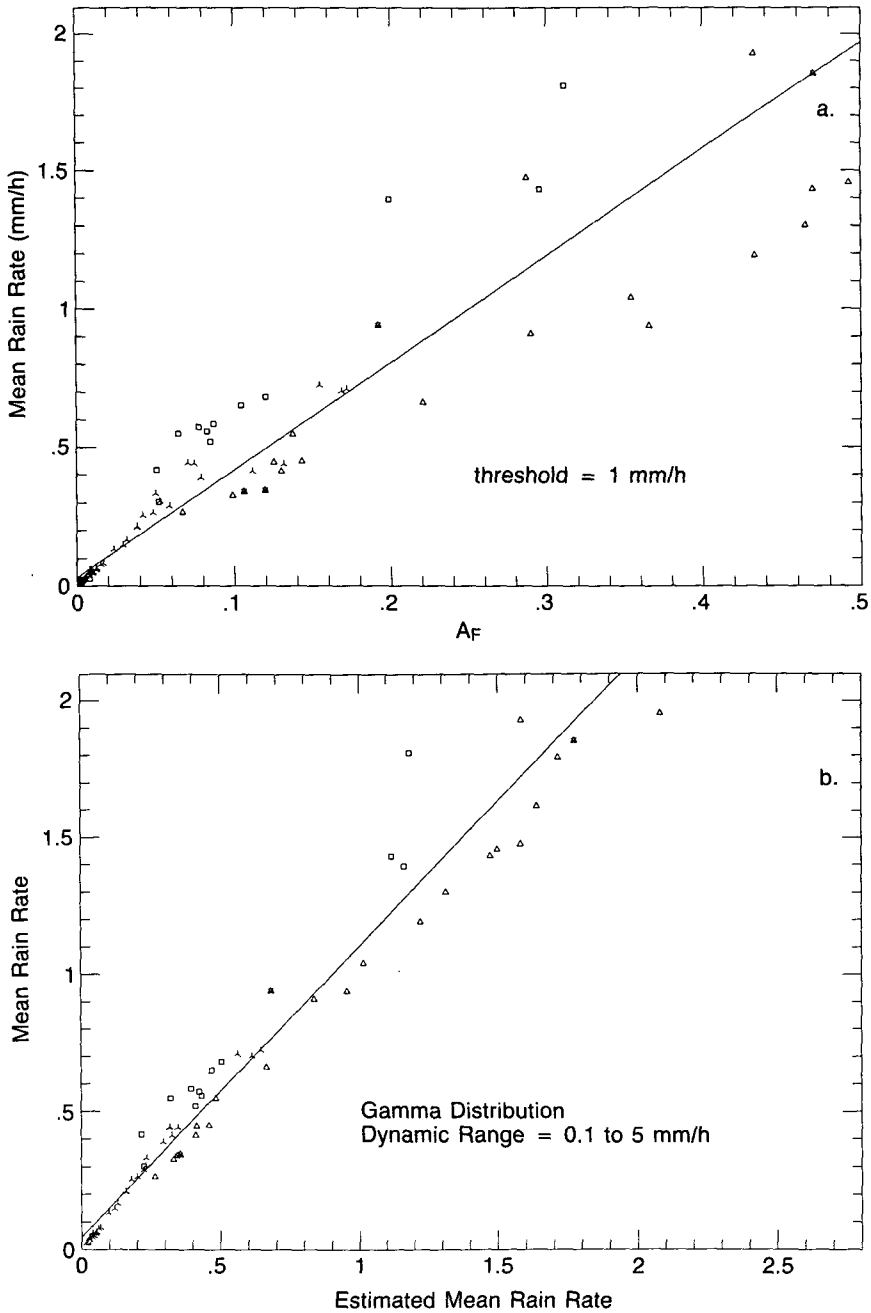

FIG. 6. Comparison of single- and multiple-threshold methods for four partitions per PPI map. (a) Area-average rain rate versus fractional area coverage for a threshold of 1 mm h^{-1}; (b) actual versus estimated average rain rate for a dynamic range from 0.1 to 5 mm h^{-1} using a gamma model function.

sor with limited dynamic range, the optimum threshold and the conversion between fractional area and rain rate could be determined by a network of raingages or by a well-calibrated radar with a wide dynamic range. Whether this threshold calibration can be extended well beyond the ground-truth network, however, is a function of how stable the relationship is in time and space.

A second limitation is that the method provides only the mean of the area rain rates. While this quantity appears to be the most important statistic in climatological studies, for applications in hydrology and in satellite communications, statistics such as the variance of the rain field and the probability of exceedance above a threshold are relevant as well.

To test the accuracy of estimating the probability of exceedance, the dynamic range is fixed at 0.5–5 mm h^{-1} and $\Pr(R > R_0)$ is calculated for the cases R_0 = 1, 5, and 10 mm h^{-1}. The results are shown in Figs. 7a–c where the lognormal model function is used. For the case shown in Fig. 7a, where R_0 = 1 mm h^{-1}, the estimates are nearly perfect, a reasonable result in the sense that the majority of rain rates exceeding 1 mm h^{-1} fall within the measurement range from 0.5 to 5 mm h^{-1}. More informative are the results in Fig. 7b, which show that the estimated values of $\Pr(R > 5$ mm $h^{-1})$ are accurate even though the rain rates in question fall outside the measurement range. As shown in Fig. 7c, however, the accuracy of the estimate of $\Pr(R > R_0)$ degrades significantly when R_0 is increased from 5 to 10 mm h^{-1}: in particular, at R_0 = 5 mm h^{-1}, the square of the correlation coefficient between the actual and estimated exceedance probability is 0.98, which decreases to 0.69 for R_0 = 10 mm h^{-1}. The estimate of $\Pr(R > 10$ mm $h^{-1})$ can be improved by broadening the dynamic range: for example, an increase in the dynamic range from 0.5–5 to 0.05–20 mm h^{-1} increases ρ^2 from 0.69 to 0.95.

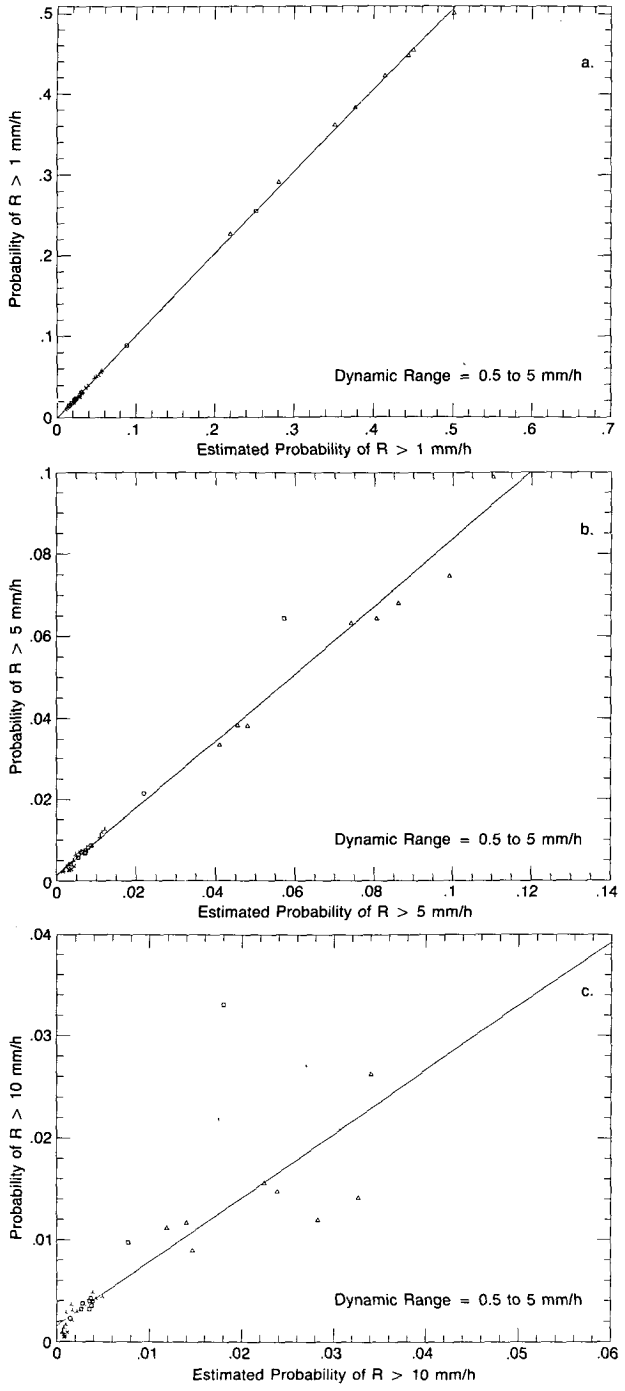

FIG. 7. Actual versus estimated probabilities of exceedance for a dynamic range of 0.5–5 mm h^{-1} using a lognormal model function with exceedance probabilities of (a) 1 mm h^{-1}; (b) 5 mm h^{-1}; and (c) 10 mm h^{-1}.

Expressions for the variance of the area rain rate are given by (5) and (8) for the lognormal and gamma models, respectively. The results of computing the standard deviation of the area rain rates over the 37 PPI maps are shown in Table 5 for the lognormal and gamma test functions. The results show that neither test function gives adequate estimates of the standard deviation. Although, in general, the lognormal yields fairly small biases, the estimates are poorly correlated with the actual values. On the other hand, the results derived from the gamma model function exhibit much higher correlations but exhibit a fairly large underestimation. The reasons for this poor performance are not known. Some understanding, and perhaps improvement in the estimates, might be gained from a larger database of PPI maps and from an examination of test functions other than the lognormal or gamma.

4. Local versus areawide methods

A number of spaceborne radar methods have been proposed for the estimation of rain parameters from space. Nearly all are applied to measurements taken over an area on the order of the instantaneous field of view (IFOV) of the instrument. In the case of the proposed Tropical Rainfall Measuring Mission (TRMM) radar, for example, the IFOV at the surface is approximately 4.5 km in diameter at nadir incidence (Okamoto 1988). For many climatological applications, however, the relevant area over which the rain is to be characterized is much larger, typically on the order (100 km)^2 (Simpson et al. 1989). The most straightforward way of computing areawide statistics is to use the local estimates as measured at each IFOV. The drawback is that the accuracy of the locally measured estimate depends on the rain rate.

Figure 8 illustrates the performance of the radar as a function of the rain rate. The length of the vertical bars represents the standard deviation of the estimate, while the center point gives the ratio of the mean of

TABLE 5. Multiple threshold statistics—standard deviation of area rain rate (N = 37).

Dynamic range (mm h^{-1})	ρ^2	MSE (mm h^{-1})	SEE (mm h^{-1})	Slope
Lognormal distribution				
0.5–1	.20	$\gg 1$	$\gg 1$	$\gg 1$
0.5–3	.63	2.00	1.44	2.02
0.5–5	.57	0.96	0.86	1.07
0.1–5	.57	0.94	0.84	1.03
0.05–20	.58	1.03	0.85	1.07
Gamma distribution				
0.5–1	.64	1.14	0.75	1.08
0.5–3	.76	0.93	0.33	0.64
0.5–5	.83	0.89	0.25	0.59
0.1–5	.83	0.87	0.25	0.60
0.05–20	.90	0.68	0.22	0.71

the estimate to the actual rain rate R_a; for example, if the center point is greater than one, the estimate is positively biased. Although the precise nature of these curves depend on the radar design and the rain estimation method that is used, the general behavior is valid for most radar designs and methods. At sufficiently light rain rates, the rain signal-to-noise ratio will be small and the rain-rate estimate will be positively biased. Conversely, at high rain rates, the estimate will be negatively biased because of attenuation effects. Between these extremes, an intermediate region usually exists where the rain rate is sufficiently high that the signal-to-noise ratio is large but not so large as to cause significant attenuation effects. This region is shown in Fig. 8 as extending from $R_{\min}$ to $R_{\max}$. To relate this somewhat more realistic model to the model used in sections 1–3, note that this optimum operating range expresses the same idea as that of the dynamic range referred to earlier. Thus, in the application of multiple thresholds—the n thresholds—$R_T(j), j = 1, \cdots, n$, would be chosen such that

$$R_T(j) = \left(\frac{j-1}{n-1}\right)(R_{\max} - R_{\min}) + R_{\min}.$$

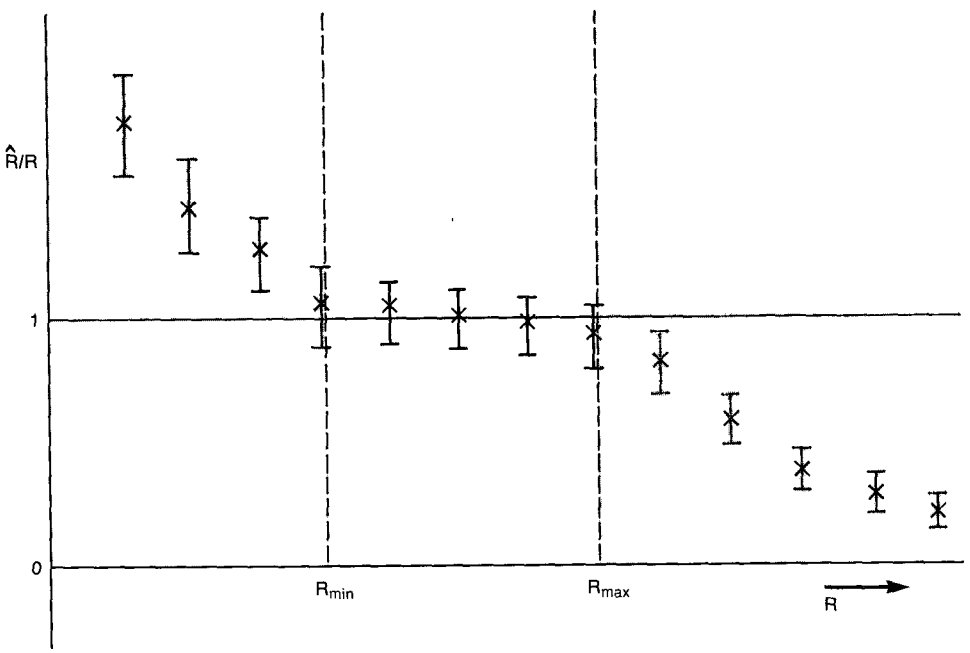

FIG. 8. Schematic of the normalized mean and standard deviation of the local rain-rate estimates versus rain rate. The effective dynamic range is chosen to extend from $R_{\min}$ to $R_{\max}$, where the bias of the estimate is relatively small.

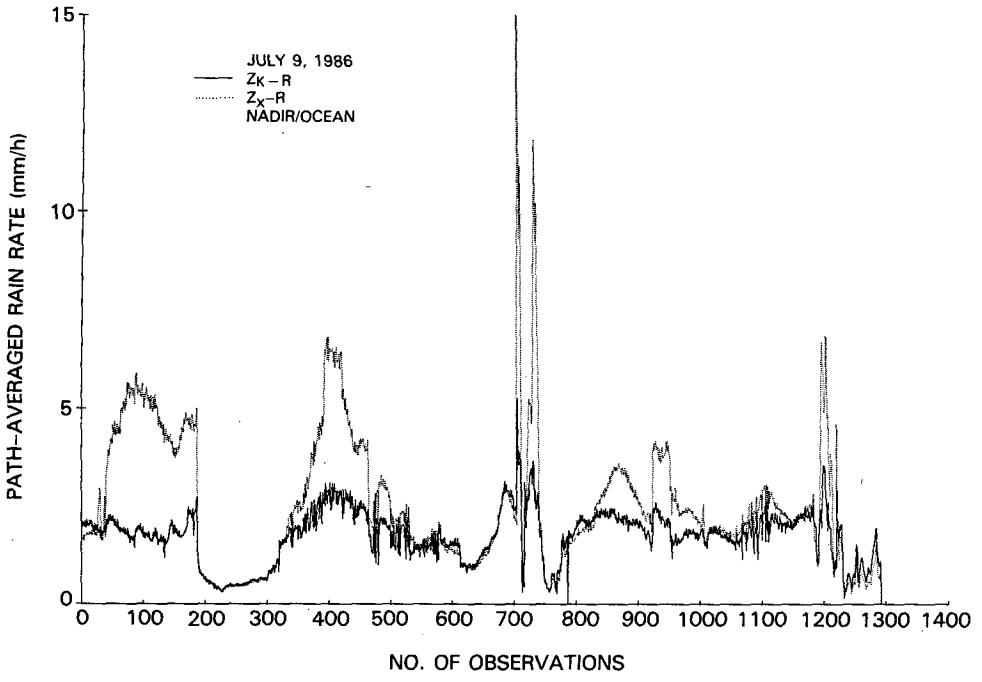

FIG. 9. Comparisons of path-averaged rain rates R versus time as determined from 10 GHz (dotted line) and 35 GHz (solid line) nadir-viewing measurements of Z and use of Z–R relationships. Each observation corresponds to a 0.5-s integration (after Meneghini et al. 1989).

Although several applications of the threshold method have been described (Atlas et al. 1990), the primary function of this technique, as interpreted in this paper, is to estimate the statistical properties of the rain field based on measurements at a single threshold or over a range of thresholds. This approach is effective if it allows us to extrapolate from a region where the local measurements are relatively accurate to regions where they are poor. If the local estimates over the measurement area are all equally accurate, or inaccurate, then thresholding offers no advantage. It follows that this kind of threshold method is useful only if the distribution of rain rates over the area in question contains rain rates both within and outside the optimum measurement interval from $R_{\min}$ to $R_{\max}$.

To illustrate a case where thresholding can be used to some advantage, consider the example in Fig. 9, which shows path-averaged estimates of rain rate as derived from Z–R relationships applied to 10-GHz (solid line) and 35-GHz (dashed line) airborne radar data (Meneghini et al. 1989). The rain rates are derived from an average of reflectivities over a 128-sample average (one observation is 0.5 s) so that the curves in Fig. 9 can be interpreted as the sequence of estimated rain rates under the aircraft flight track. While the two estimates agree well for rain rates below about 3 mm h^{-1}, above this value, the 35-GHz results clearly show a saturation effect caused by attenuation. An average over these local estimates at 35 GHz would yield a negatively biased result. On the other hand, the use of multiple thresholds from a light rain rate to about 3 mm h^{-1} or a single threshold between 1 and 3 mm h^{-1} should give a more accurate estimate of the mean rain rate. For the 10-GHz data, where the signal strength is large and the attenuation effects are fairly small, the use of thresholds would afford no advantage unless additional information were available on the relative accuracy of the estimate as a function of rain rate.

5. Other error sources

For the quantitative results presented in sections 3 and 4, an idealized model of the radar performance was assumed where the only source of error arises from the finite dynamic range of the instrument. In this section, other sources of error are discussed qualitatively.

In the application of the threshold method to the airborne data shown in Fig. 9, the quantity used to estimate the path-averaged rain rate is a monotonic function of rain rate; in particular, if a Z–R law ($R_j = aZ_j^b$) is used to convert the measured reflectivity factor at the jth range gate, Z_j, to a rain rate R_j, the path-averaged estimate is given by

$$\frac{1}{n}\sum_{j=1}^{n} aZ_j^b.$$

This estimate, which approaches a limit asymptotically as the rain rate increases, is a monotonic of function of the path-averaged rain rate. Techniques such as the surface reference and the dual wavelength are also

monotonic functions of the path-averaged rain rate. This characteristic of the estimator allows the application of thresholding methods (single and multiple) as long as threshold values are not taken near the upper limit. This situation is in contrast to methods where the estimator is double valued; the most obvious case is the rain rate derived from the measured reflectivity factor in the presence of attenuation.[2] In cases where the estimator is double valued, the threshold methods are unreliable since they assign, in effect, large and small rain rates to a single category.

With respect to radar calibration errors and errors in the Z–R laws, the single- and multiple-threshold methods are nearly the same. For example, if the high-resolution estimates of rain rate are biased by a certain amount, the area-average rain rates derived from either threshold method will be biased by the same amount. The effects of errors in the Z–R law caused by fluctuations in the drop-size distribution (DSD) are somewhat more complicated, and it is helpful to make a distinction between variations of the DSD about the area-averaged DSD and the bias between the actual and assumed area-averaged DSDs. Because of the area averages that are taken in applying the threshold methods, the random error will be almost completely eliminated while the bias will remain.

The final source of error that will be mentioned is the partial beam-filling problem. A quantitative analysis of this problem is beyond the scope of this paper (Nakamura 1991); only a brief qualitative discussion is given here. Some insight into this question can be gained by considering an extreme case where the radar beamwidth is as large as the area average to be computed [i.e., on the order of (100 km)^2]. We assume, moreover, that the radar has infinite sensitivity and that the relationship between the measured reflectivity factor and rain rate is linear. Because of the large spatial average, the variance of the distribution will narrow considerably and the cumulative distribution function (conditioned on rain being present) will approximate a step function with a sharp transition from zero to one at the climatological mean rain rate. For this case, at least two threshold measurements are needed (one on either side of the discontinuity) since a single-threshold measurement will capture either all or none of the area. However, if the discontinuity can be located accurately, then because of the linear relationship between Z and R, the exact area-average rain rate can be recovered. Of course, for most DSDs, the Z–R relationship is nonlinear so that the assumption of uniform beam filling will produce estimates of R that are positively biased. Thus, although the actual area-averaged rain rates should be tightly clustered about the climatological mean, the inferred distribution will be slightly broadened (the larger variance being caused by changes in the Z–R law) and positively biased (due to the nonlinear Z–R law).

6. Summary

In this paper, a multiple-threshold approach has been described and analyzed. The method relies on the fact that the fractional area above a certain rain-rate threshold R_T is directly related to the distribution of the area-average rain rate at that threshold value. This implies that a sensor that accurately measures the rain rate from R_{min} to R_{max} provides estimates of the distribution function over this range. To obtain the distribution at all rain rates, a model function such as the lognormal or gamma is chosen with the unknown parameters adjusted so that the mean-square error between the test function and the measured values of the distribution is minimized. Once the unknown parameters are obtained, any first-order statistic of the area-wide rain rate can be found.

To test this approach, PPI maps from the SPANDAR radar were used to simulate examples of the true rain-rate field. The simple error model used to evaluate the method is that the sensor is able to measure the rain rate perfectly over a finite dynamic range of rain rates. Results are presented giving the accuracy of the method as a function of 1) the dynamic range of the instrument; 2) the model function that is used (lognormal and gamma); and 3) the size of the averaging area. Comparisons between this and the single-threshold method indicate that the use of multiple thresholds is more accurate only if the dynamic range of the instrument is sufficiently broad. When this condition is met, the multiple-threshold approach has the advantage that an independent calibration (converting fractional area to area-average rain rate) is not required. Moreover, because the distribution function itself is estimated, any first-order statistic can be computed.

The use of thresholding, as interpreted in this paper, is beneficial only if it provides results more accurate than a straightforward computation based on locally derived rain rates. Necessary conditions are that the rain rate estimator be single valued and be more accurate over a particular range of rain rates than outside this range. These conditions appear to be satisfied in the case of a high-frequency spaceborne radar (e.g., 35 or 95 GHz), where the effective dynamic range of the instrument is severely limited by attenuation even when a combination of backscattering and attenuation methods are used. To understand the relationship between local and global methods in a more quantitative way, however, will require the simulation of both types of approach within the context of a more realistic error model.

Acknowledgments. We would like to thank Norris Beasley and the rest of the SPANDAR crew for pro-

[2] Although the summation of the Z_j over the path is a monotonic function of the path-averaged rain rate, this quantity at a single range gate is, in general, a double-valued function of the rain rate.

viding the radar data and David Atlas for his suggestions and comments.

REFERENCES

Atlas, D., D. Rosenfeld, and D. A. Short, 1990: The estimation of convective rainfall by area integrals. Part I: The theoretical and empirical basis. *J. Geophys. Res.*, **95,** 2153–2160.

Byers, H. R., 1948: The use of radar in determining the amount of rain falling over a small area. *Trans. Amer. Geophys. Union,* **29,** 187–196.

Chiu, L. S., 1988: Rain estimation from satellites: Areal rainfall–rain area relations. Preprints, *Third Conf. on Satellite Meteorology and Oceanography,* Anaheim, Amer. Meteor. Soc., 363–368.

Doneaud, A. A., S. I. Niscov, D. L. Priegnitz, and P. L. Smith, 1984: The area–time integral as an indicator for convective rain volumes. *J. Climate Appl. Meteor.*, **23,** 555–561.

Kedem, B., L. S. Chiu, and Z. Karni, 1990: An analysis of the threshold method for measuring area average rainfall. *J. Appl. Meteor.*, **29,** 3–20.

Meneghini, R., K. Nakamura, C. W. Ulbrich, and D. Atlas, 1989: Experimental tests of methods for the measurement of rainfall using an airborne dual-wavelength radar. *J. Atmos. Oceanic Technol.*, **6,** 637–651.

Nakamura, K., 1991: Biases of rain retrieval algorithms for spacebo:ne radar caused by nonuniformity of rain. *J. Atmos. Oceanic Technol.*, **8,** 363–373.

Okamoto, K., J. Awaka, and T. Kozu, 1988: A feasibility study of rain radar for the Tropical Rainfall Measuring Mission: 6. A case study of rain radar system. *J. Comm. Research Lab.*, **35,** 183–208.

Papoulis, A., 1965: *Probability, Random Variables, and Stochastic Processes.* McGraw-Hill, 583 pp.

Rosenfeld, D., D. Atlas, and D. A. Short, 1990: The estimation of convective rainfall by area integrals. Part II: The height–area threshold (HART) method. *J. Geophys. Res.*, **95,** 2161–2176.

Short, D. A., D. B. Wolff, D. Rosenfeld, and D. Atlas, 1993: A study of the threshold method utilizing raingage data. *J. Appl. Meteor.*, **32,** in press.

Simpson, J., R. F. Adler, and G. North, 1988: A proposed Tropical Rainfall Measuring Mission (TRMM) satellite. *Bull. Amer. Meteor. Soc.*, **69,** 278–295.